

Sampling in Unit Time with Kernel Fisher–Rao Flow

Aimee Maurais & Youssef Marzouk
 Center for Computational Science and Engineering
 Massachusetts Institute of Technology
 Cambridge, MA 02139
 {maurais, ymarz}@mit.edu

Abstract

We introduce a new mean-field ODE and corresponding interacting particle systems (IPS) for sampling from an unnormalized target density. The IPS are gradient-free, available in closed form, and only require the ability to sample from a reference density and compute the (unnormalized) target-to-reference density ratio. The mean-field ODE is obtained by solving a Poisson equation for a velocity field that transports samples along the geometric mixture of the two densities, $\pi_0^{1-t}\pi_1^t$, which is the path of a particular Fisher–Rao gradient flow. We employ a RKHS ansatz for the velocity field, which makes the Poisson equation tractable and enables discretization of the resulting mean-field ODE over finite samples. The mean-field ODE can additionally be derived from a discrete-time perspective as the limit of successive linearizations of the Monge–Ampère equations within a framework known as sample-driven optimal transport. We introduce a stochastic variant of our approach and demonstrate empirically that our IPS can produce high-quality samples from varied target distributions, outperforming comparable gradient-free particle systems and competitive with gradient-based alternatives.

1 Introduction

In this work we consider the problem of *sampling via transport*: given a target distribution π_1 on \mathbb{R}^d and a reference distribution π_0 on \mathbb{R}^d from which we can sample, our goal is to find $T : \mathbb{R}^d \rightarrow \mathbb{R}^d$ such that $T_\# \pi_0 = \pi_1$, i.e., $X_0 \sim \pi_0 \Rightarrow T(X_0) \sim \pi_1$. We assume that π_0 and π_1 both admit densities and that we can evaluate the (unnormalized) *density ratio*¹ $\frac{\pi_1}{\pi_0}$ but that we do not have samples of π_1 with which to train the map or access to gradients, including scores, of π_1 or π_0 . The density ratio is available when the density of π_1 is known and π_0 is chosen to be some “standard” reference (e.g., Gaussian), but is also accessible in the Bayesian setting so long as the likelihood function is known: therein $\pi_1 \propto \ell \pi_0$ for some likelihood $\ell(x) = \pi(y^*|x)$, and hence the ratio is $\frac{\pi_1}{\pi_0} \propto \ell$. We thus use the term “likelihood” to refer to the ratio $\frac{\pi_1}{\pi_0}$ throughout this paper.

The canonical sampling approach employing the likelihood is importance sampling [43], which transforms an unweighted ensemble of samples of π_0 into a *weighted* ensemble, enabling the estimation of expectations under π_1 . Importance sampling is the foundation for sequential Monte Carlo (SMC) methods [16], but is frequently plagued by issues of weight degeneracy and ensemble collapse, necessitating large ensemble sizes [52] or interventions such as resampling [34] and MCMC rejuvenation.

Alternatively, many sampling approaches use *dynamics* to define a transport incrementally, e.g., via the flow map induced by trajectories of an ODE or the stochastic mapping induced by sample

¹For the remainder of this paper, the terms “density” and “density ratio” refer to unnormalized quantities unless otherwise stated.

paths of an SDE. In either case, the idea is to apply dynamics which will transform some initial state $X_0 \sim \pi_0$ to a state $X_S \sim \pi_{X_S} \approx \pi_1$ for some time $S > 0$. This approach underlies flow, diffusion, and bridge techniques for generative modeling, e.g., [33, 53, 15, 38, 36, 65, 1], wherein samples from both π_0 and π_1 are almost always required for training (with [62, 27] being recent exceptions). In the setting where π_1 is known only through its unnormalized density, there are a number of dynamic sampling algorithms which have their grounding as *gradient flows* of functionals on spaces of probability measures. There are several geometries in which one may define gradient flows on probability measures (see [10] for a helpful review), but most well-known algorithms in this vein (e.g., [37, 22, 23, 48]) use some form of the Wasserstein geometry [63] to define dynamics which must, in principle, be run for *infinite time* in order to ensure correct sampling from π_1 .

In this work we develop a dynamic sampling approach based on an ODE which transports samples from π_0 to π_1 in *unit time* such that the time-dependent distribution of the samples is the geometric mixture $\pi_t \propto \pi_0^{1-t} \pi_1^t = \pi_0 \left(\frac{\pi_1}{\pi_0}\right)^t$, $t \in [0, 1]$. Although our algorithms are gradient-free and only require the likelihood $\frac{\pi_1}{\pi_0}$, the path of distributions π_t corresponds to the Fisher–Rao gradient flow of the expected negative log likelihood. The underlying dynamics are described by a **mean-field ODE model**, which we show is the limit of two different **interacting particle systems**. These interacting particle systems, which we generally refer to as *Kernel Fisher–Rao Flow*, are obtained in two distinct but related ways. On one hand, in continuous time, the mean-field ODE can be obtained from the weak formulation of a Poisson equation for a *velocity field* defined in a reproducing kernel Hilbert space (RKHS), from which we obtain a finite-particle ODE system by approximating expectations via Monte Carlo (Section 3). On the other, in discrete time, one can approximate the optimal transport map which pushes π_t to $\pi_{t+\Delta t}$ via linearization of the Monge–Ampère equations discretized over finitely many kernel basis functions and finitely many samples (Section 4). This linearization yields an interacting particle system which in discrete time is distinct from, but in continuous time identical to, that obtained via the RKHS approach to Poisson’s equation.

2 Background

Sampling via measure transport is an active area of research, with many computational approaches [39, 31, 44, 61] appearing in recent years. Most practical transport maps are parameterized, and thus a crucial part of realizing them is selecting an appropriately rich function class within which to search for the map. Common map approximation classes include polynomials [29], radial basis functions [55], composed simple transformations [49, 31, 44], neural networks [8, 58, 3], and reproducing kernel Hilbert spaces [37, 33, 30]. Determining an appropriate basis to represent a transport map can be challenging, especially when the target and reference distributions are high-dimensional or differ from each other considerably. For this reason it may be necessary to employ, e.g., adaptive feature selection algorithms [4] or dimension reduction techniques [54, 9, 7, 12].

As an alternative to searching for a single, potentially highly complex transport map which pushes the reference π_0 directly to the target π_1 , one can instead prescribe a *path* of distributions $(\pi_t)_{t \in [0,1]}$ having the target and reference as endpoints and seek a sequence of maps T_1, \dots, T_N which push samples along a discretization of the path, as depicted in Figure 1. The composed map $T = T_N \circ T_{N-1} \circ \dots \circ T_1$ pushes forward π_0 to π_1 . In continuous time this approach becomes one of finding a *velocity field* $v_t : \mathbb{R}^d \rightarrow \mathbb{R}^d$ such that the solution to the initial value problem

$$\dot{X}_t = v_t(X_t), \quad X_0 \sim \pi_0$$

has distribution π_t . Samplers of unnormalized densities which employ this homotopy approach frequently take π_t to be the geometric mixture

$$\pi_t \propto \pi_0^{1-t} \pi_1^t = \pi_0 \left(\frac{\pi_1}{\pi_0}\right)^t, \quad t \in [0, 1], \quad (1)$$

which interpolates between π_0 and π_1 in unit time. This mixture may be referred to as the “power posterior” path and appears, for example, in annealed importance sampling [41, 5, 32, 26] and parallel tempering [24, 20, 57]. In Bayesian computation, this path is sometimes referred to as “tempered likelihood” and has been used as the basis for algorithms which generate (approximate) posterior samples [46, 14, 28, 18] or posterior densities [17].

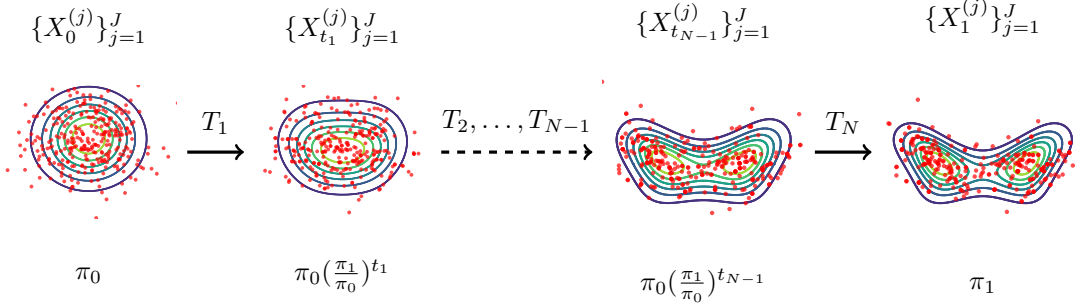


Figure 1: We employ a homotopy-based sampling scheme in this work, deriving a mean-field ODE which approximately transports a reference π_0 to a target π_1 in unit time. In discrete time this approach amounts to obtaining incremental transport maps T_1, \dots, T_N .

2.1 Related work

The idea of using dynamics with the tempered likelihood to sample the posterior distribution in Bayesian inference was, to our knowledge, first developed by Daum and Huang [13] and Reich [46] in the context of filtering. In Daum and Huang [13, 14] and related works by the same authors, the tempered likelihood is used to derive ODEs and SDEs for nonlinear filtering in full generality, and as such these systems require gradients and even Hessians of the likelihood and prior. The algorithms for propagating samples from prior to posterior along the tempered likelihood in Reich [46] are of ensemble-Kalman type and employ a Gaussian approximation for each π_t , meaning that their expressivity is limited. A similar methodology to [46], now known as Ensemble Kalman Inversion (EKI), was proposed for computing point estimates in Bayesian inverse problems in Iglesias et al. [28]. The iteration underlying EKI is run for infinite time, but, as noted by, e.g., Ding and Li [18], when the iteration is stopped at $t = 1$ samples from an approximation to the posterior are obtained. Even in the limit of infinite particles and continuous time, however, ensemble Kalman methods are not consistent samplers for general (i.e., non-Gaussian) posteriors.

The tempered likelihood path is frequently employed in sequential Monte Carlo (SMC) methods, which rely on a series of interwoven importance re-sampling and mutation steps to gradually transform samples from π_0 into approximate samples from π_1 . Several recent works have sought to use transport within SMC to either replace or reduce the frequency of multinomial resampling. The basic idea, which was introduced in Reich [47] and which motivates our development in Section 4, is to use importance weights to obtain a transport between π_t and $\pi_{t+\Delta t}$. In Ruchi et al. [50, 51] and Myers et al. [40], discrete optimal transport couplings are used to define linear transformations which replace the importance resampling steps typically employed in SMC. In a similar vein, the annealed flow transport Monte Carlo of Arbel et al. [2] uses transport as a preconditioner for SMC; on each SMC iteration a parametric transport map between π_t and $\pi_{t+\Delta t}$ is learned and applied to samples from π_t before the standard resampling and mutation steps are performed. In each of these works the transport steps remain embedded within SMC schemes, while our algorithms are based on dynamics and do not require resampling or application of mutation kernels.

Concurrently with our work, Wang and Nüsken [64] developed very similar mean-field ODE systems and algorithms for transporting samples along the tempered likelihood. Their algorithms are motivated from a kernel mean embedding perspective, rather than one of optimal transport and Fisher–Rao gradient flows, and can be made to match ours by specifying particular choices of the parameters v_t^0 and C_t in their setup. In our work we introduce both deterministic and stochastic interacting particle systems for sampling the tempered likelihood, but the algorithms considered in Wang and Nüsken [64] are purely deterministic.

Notation We use $K(\cdot, \cdot) : \mathbb{R}^d \times \mathbb{R}^d \rightarrow \mathbb{R}$ to represent a symmetric positive definite kernel on \mathbb{R}^d and denote by $(\mathcal{H}_K, \langle \cdot, \cdot \rangle_{\mathcal{H}_K})$ the reproducing kernel Hilbert space [56] associated with K . We assume that $K(\cdot, x)$ is C^2 and use $\nabla_1 K(\cdot, \cdot)$ to refer to the gradient of K with respect to the first argument and $\nabla_2 K(\cdot, \cdot)$ to refer to the gradient with respect to the second. $\mathcal{P}_{2,ac}(\mathbb{R}^d)$ denotes the space of probability measures on \mathbb{R}^d with finite second moments and which admit densities.

3 Methodology: Poisson's equation in reproducing kernel Hilbert space

Our goal is to find a time-varying velocity field $v_t : \mathbb{R}^d \rightarrow \mathbb{R}^d$ such that the distribution of X_t evolving according to

$$\dot{X}_t = v_t(X_t), \quad X_0 \sim \pi_0 \quad (2)$$

is the geometric mixture (1). Had we access to such a velocity field, we could obtain samples from π_1 by sampling π_0 and simulating the dynamics (2) for unit time. It can be shown that π_t in (1) satisfies

$$\partial_t \pi_t = \pi_t \left(\log \frac{\pi_1}{\pi_0} - \mathbb{E}_{\pi_t} \left[\log \frac{\pi_1}{\pi_0} \right] \right),$$

which is the Fisher–Rao gradient flow of the functional $\mathcal{F} : \mathcal{P}_{2,ac}(\mathbb{R}^d) \rightarrow \mathbb{R}$ defined

$$\mathcal{F}(\pi) = -\mathbb{E}_{\pi} \left[\log \frac{\pi_1}{\pi_0} \right].$$

$\mathcal{F}(\pi)$ is the expected negative log likelihood under π . Using the continuity equation, a velocity field in (2) yielding $X_t \sim \pi_t$ must then satisfy

$$-\nabla \cdot (\pi_t v_t) = \pi_t \left(\log \frac{\pi_1}{\pi_0} - \mathbb{E}_{\pi_t} \left[\log \frac{\pi_1}{\pi_0} \right] \right). \quad (3)$$

There are many possible solutions to the PDE (3), but if, as in [59, 46], we insist that in the limit $\Delta t \rightarrow 0$ the expected transportation cost $\frac{1}{\Delta t^2} \mathbb{E}_{\pi_t} [\|X_t - X_{t+\Delta t}\|^2]$ is minimized for each t , we obtain a constrained optimization problem for each v_t with a unique solution,

$$\min_{v_t : \mathbb{R}^d \rightarrow \mathbb{R}^d} \int_{\mathbb{R}^d} \|v_t\|^2 d\pi_t \quad \text{s.t.} \quad -\nabla \cdot (\pi_t v_t) = \pi_t \left(\log \frac{\pi_1}{\pi_0} - \mathbb{E}_{\pi_t} \left[\log \frac{\pi_1}{\pi_0} \right] \right).$$

It can be shown by calculus of variations [46] that the optimal solution to this problem is $v_t = \nabla u_t$, where u_t satisfies the Poisson equation

$$-\nabla \cdot (\pi_t \nabla u_t) = \pi_t \left(\log \frac{\pi_1}{\pi_0} - \mathbb{E}_{\pi_t} \left[\log \frac{\pi_1}{\pi_0} \right] \right). \quad (4)$$

We make (4) tractable by searching for u_t in the RKHS \mathcal{H}_K , i.e., taking $u_t(\cdot) = \int_{\mathbb{R}^d} K(\cdot, x) f_t(x) d\pi_t(x)$ for some $f_t : \mathbb{R}^d \rightarrow \mathbb{R}$, and enforcing the weak form of (4), as in [35], for kernel test functions $K(\cdot, x)$,

$$\int_{\mathbb{R}^d} \langle \nabla_1 K(y, x), \nabla u_t(y) \rangle d\pi_t(y) = \int_{\mathbb{R}^d} K(y, x) \left(\log \frac{\pi_1}{\pi_0}(y) - \mathbb{E}_{\pi_t} \left[\log \frac{\pi_1}{\pi_0} \right] \right) d\pi_t(y) \quad \forall x \in \mathbb{R}^d. \quad (5)$$

We require (5) to hold for all $x \in \mathbb{R}^d$. Substituting the form of u_t into (5), we have

$$\begin{aligned} \iint_{\mathbb{R}^d \times \mathbb{R}^d} f_t(z) \langle \nabla_1 K(y, x), \nabla_1 K(y, z) \rangle d\pi_t(y) d\pi_t(z) \\ = \int_{\mathbb{R}^d} K(x, y) \left(\log \frac{\pi_1}{\pi_0}(y) - \mathbb{E}_{\pi_t} \left[\log \frac{\pi_1}{\pi_0} \right] \right) d\pi_t(y). \end{aligned} \quad (6)$$

We write the relationship (6) succinctly as $M_{\pi_t} f_t(x) = K_{\pi_t} (\log \frac{\pi_1}{\pi_0} - \mathbb{E}_{\pi_t} [\log \frac{\pi_1}{\pi_0}])(x)$, where the integral operator M_{π_t} maps functions $g : \mathbb{R}^d \rightarrow \mathbb{R}$ to

$$\begin{aligned} M_{\pi_t} g(\cdot) &= \int_{\mathbb{R}^d} g(z) \mathbb{E}_{X_t \sim \pi_t} [\langle \nabla_1 K(X_t, \cdot), \nabla_1 K(X_t, z) \rangle] d\pi_t(z) \\ &= \iint_{\mathbb{R}^d \times \mathbb{R}^d} g(z) \langle \nabla_1 K(y, x), \nabla_1 K(y, z) \rangle d\pi_t(y) d\pi_t(z) \end{aligned}$$

and the kernel integral operator K_{π_t} maps g to $K_{\pi_t} g(\cdot) = \int_{\mathbb{R}^d} g(z) K(\cdot, z) d\pi_t(z)$. Under the condition that M_{π_t} is invertible, f_t is given by $f_t(\cdot) = M_{\pi_t}^{-1} K_{\pi_t} \left(\log \frac{\pi_1}{\pi_0} - \mathbb{E}_{\pi_t} \left[\log \frac{\pi_1}{\pi_0} \right] \right)$ and we have $v_t(\cdot) = \nabla u_t(\cdot)$ equal to

$$v_t(\cdot) = \int_{\mathbb{R}^d} \nabla_1 K(\cdot, x) M_{\pi_t}^{-1} K_{\pi_t} \left(\log \frac{\pi_1}{\pi_0} - \mathbb{E}_{\pi_t} \left[\log \frac{\pi_1}{\pi_0} \right] \right)(x) d\pi_t(x). \quad (7)$$

Therefore, starting from $X_0 \sim \pi_0$ the **mean-field ODE**

$$\dot{X}_t = v_t(X_t) = \mathbb{E}_{\rho_t} \left[\nabla_1 K(X_t, X') M_{\rho_t}^{-1} K_{\rho_t} \left(\log \frac{\pi_1}{\pi_0} - \mathbb{E}_{\rho_t} \left[\log \frac{\pi_1}{\pi_0} \right] \right) (X') \right], \quad (8)$$

can be used to evolve samples from π_0 such that $\rho_t = \text{Law}(X_t)$ is approximately $\pi_t \propto \pi_0^{1-t} \pi_1^t$, and hence at $t = 1$ they are approximately distributed as π_1 .

We note that the potential u_t obtained by solving a weak-form Poisson equation over the RKHS,

$$u_t = \int_{\mathbb{R}^d} K(\cdot, x) M_{\pi_t}^{-1} K_{\pi_t} \left(\log \frac{\pi_1}{\pi_0} - \mathbb{E}_{\pi_t} \left[\log \frac{\pi_1}{\pi_0} \right] \right) (x) d\pi_t(x)$$

is not necessarily a strong solution to (4). For this reason we differentiate between the target path of distributions $\pi_t \propto \pi_0^{1-t} \pi_1^t$ and $\rho_t = \text{Law}(X_t)$. Understanding the difference between these paths and its dependence on the choice of RKHS \mathcal{H}_K is an important area for future work. Empirically we find the quality of samples generated by running a discretization of (8) to be good; see Section 6.

Because the quantities appearing in v_t can be written as expectations with respect to ρ_t , the mean-field model (8) can be approximated for finite samples as an **interacting particle system**.

Theorem 1 *Consider the interacting particle system*

$$\begin{aligned} \dot{X}_t^{(j)} &= \left(\nabla_1 K(X_t^{(j)}, X_t^{(1)}) \quad \dots \quad \nabla_1 K(X_t^{(j)}, X_t^{(J)}) \right) M_t^{-1}. \\ &\quad \frac{1}{J} \sum_{k=1}^J \left(\log \frac{\pi_1}{\pi_0}(X_t^{(k)}) - \frac{1}{J} \sum_{i=1}^J \log \frac{\pi_1}{\pi_0}(X_t^{(i)}) \right) \begin{pmatrix} K(X_t^{(k)}, X_t^{(1)}) \\ \vdots \\ K(X_t^{(k)}, X_t^{(J)}) \end{pmatrix}, \quad j = 1, \dots, J \end{aligned} \quad (9)$$

with $t \in [0, 1]$, $\{X_0^{(j)}\}_{j=1}^J \stackrel{\text{i.i.d.}}{\sim} \pi_0$, and $M_t \in \mathbb{R}^{J \times J}$ given by

$$(M_t)_{\ell, m} = \frac{1}{J} \sum_{i=1}^J \langle \nabla_1 K(X_t^{(i)}, X_t^{(\ell)}), \nabla_1 K(X_t^{(i)}, X_t^{(m)}) \rangle, \quad \ell, m = 1, \dots, J.$$

The limit of (9) as $J \rightarrow \infty$ is the mean-field ODE (8).

Proof: See Appendix A.1

We refer to the interacting particle system (9) as **Kernel Fisher–Rao Flow (KFRFlow)** and offer a few observations:

- We only require the abilities to sample π_0 and compute the log density ratio $\log \frac{\pi_1}{\pi_0}$ in order to simulate the ODE (9). In particular contrast to most Langevin-based algorithms [37, 23, 48], we do not require gradients, including scores, of π_0 or π_1 .
- KFRFlow is a simple, closed-form ODE and does not require use of numerical optimization to estimate a score or velocity field, in contrast to many comparable finite-time dynamic sampling algorithms [62, 36, 1, 53, 31].
- Similarly to SVGD [37], which can be viewed as a Wasserstein gradient flow with kernelized velocity field, KFRFlow is deterministic and can be viewed as a Fisher–Rao gradient flow with kernelized velocity field.
- M_t is the finite-particle analogue of M_{π_t} . A necessary condition for invertibility of M_t , $J \leq dJ$, is satisfied by construction in the IPS (9). This fact can be seen by noting that $M_t = \frac{1}{J} \sum_{i=1}^J \nabla \mathbf{K}_t(X_t^{(i)}) \nabla \mathbf{K}_t(X_t^{(i)})^\top$, where $\mathbf{K}_t : \mathbb{R}^d \rightarrow \mathbb{R}^J$ is the concatenation $\mathbf{K}_t(\cdot) = (K(\cdot, X_t^{(1)}), \dots, K(\cdot, X_t^{(J)}))^\top$ and $\nabla \mathbf{K}_t \in \mathbb{R}^{J \times d}$ is the Jacobian of \mathbf{K}_t .

Although the mean-field ODE model (8) can evocatively be viewed as resulting from the kernelization of a Fisher–Rao gradient flow, it can be recovered separately as the limit of a *discrete-time* interacting particle system obtained using sample-driven optimal transport [33]. We discuss this perspective in the following section.

4 Discrete-time interpretation: sample-driven optimal transport

In discrete time, the problem of finding a velocity field v_t such that the flow $\dot{X}_t = v_t(X_t)$ has distribution $\pi_t \propto \pi_0^{1-t} \pi_1^t$ becomes one of finding transport maps T_1, \dots, T_N which push samples from π_0 along a discretization of π_t . While we can obtain such maps by discretizing the IPS (9), for example taking $X_{t+\Delta t} = X_t + \Delta t \cdot v_t(X_t)$, we can alternately search for the maps *directly* via a framework introduced as sample-driven optimal transport in Trigila and Tabak [60], Kuang and Tabak [33], modified for our setting in which target samples are unavailable.

Suppose that at time $t \in [0, 1)$ we have samples $\{X_t^{(j)}\}_{j=1}^J \sim \pi_t$ which we would like to push forward to $\pi_{t+\Delta t} \propto \pi_t(\frac{\pi_1}{\pi_0})^{\Delta t}$. Given that π_t and $\pi_{t+\Delta t}$ both admit densities, there are many maps $T : \mathbb{R}^d \rightarrow \mathbb{R}^d$ satisfying $T_{\#}\pi_t = \pi_{t+\Delta t}$. The optimal transport approach [63], which we will approximate, is to seek the map which minimizes expected transport cost,

$$\min_{T_{\#}\pi_t = \pi_{t+\Delta t}} \mathbb{E}_{\pi_t} [\|T(X_t) - X_t\|^2]. \quad (10)$$

Owing to the choice of quadratic cost, it can be shown that the optimal map in (10) is the unique convex gradient which pushes forward π_t to $\pi_{t+\Delta t}$ [6]. That is, if we find $T = \nabla \phi$ satisfying $T_{\#}\pi_t = \pi_{t+\Delta t}$ with $\phi : \mathbb{R}^d \rightarrow \mathbb{R}$ convex, we have found the optimal transport map. Thus, we can search for the optimal transport map by seeking $\phi : \mathbb{R}^d \rightarrow \mathbb{R}$ convex such that $\nabla \phi_{\#}\pi_t = \pi_{t+\Delta t}$. The push-forward condition $\nabla \phi_{\#}\pi_t = \pi_{t+\Delta t}$ can be written as a Monge–Ampère PDE [21]

$$\pi_{t+\Delta t}(\nabla \phi(x)) \det(H_{\phi}(x)) = \pi_t(x),$$

where H_{ϕ} is the Hessian of ϕ , and interpreted in weak form as for all $f : \mathbb{R}^d \rightarrow \mathbb{R}$ continuous we have

$$\int_{\mathbb{R}^d} f(\nabla \phi(x)) d\pi_t(x) = \int_{\mathbb{R}^d} f(y) d\pi_{t+\Delta t}(y). \quad (11)$$

Given that we only have finitely many samples of π_t and access to the ratio $\frac{\pi_1}{\pi_0}$, we arguably do not have enough information to find a map $T = \nabla \phi$ which exactly satisfies $T_{\#}\pi_t = \pi_{t+\Delta t}$. Thus we apply a Galerkin approximation to (11) over a basis of kernel test functions located at each particle, $\{K(\cdot, X_t^{(j)}) : j = 1, \dots, J\}$, seeking a map

$$\nabla \phi_{\mathbf{s}}(x) = x + \sum_{j=1}^J s_j \nabla_1 K(\cdot, X_t^{(j)}), \quad (12)$$

and discretizing the weak form (11) with

$$\int_{\mathbb{R}^d} K(\nabla \phi_{\mathbf{s}}(x), X_t^{(j)}) d\pi_t(x) = \int_{\mathbb{R}^d} K(y, X_t^{(j)}) d\pi_{t+\Delta t}(y), \quad j = 1, \dots, J. \quad (13)$$

Approximating the LHS of (13) via Monte Carlo and the RHS with self-normalized importance sampling, we seek map coefficients $\mathbf{s} = (s_1, \dots, s_m)$ such that

$$\frac{1}{J} \sum_{j=1}^J \mathbf{K}_t(\nabla \phi_{\mathbf{s}}(X_t^{(j)})) = \sum_{j=1}^J w_t^{(j)} \mathbf{K}_t(X_t^{(j)}), \quad w_t^{(j)} = \frac{(\frac{\pi_1}{\pi_0}(X_t^{(j)}))^{\Delta t}}{\sum_{i=1}^J (\frac{\pi_1}{\pi_0}(X_t^{(i)}))^{\Delta t}}, \quad (14)$$

with $\mathbf{K}_t(\cdot) = (K(\cdot, X_t^{(1)}), \dots, K(\cdot, X_t^{(J)}))^{\top}$ as before. Kuang and Tabak [33] refer to the relationship (14) as *sample equivalence* and denote it by $\{\nabla \phi_{\mathbf{s}}(X_t^{(j)})\}_{j=1}^J \sim \{w_t^{(j)} X_t^{(j)}\}_{j=1}^J$. Because we have discretized the Monge–Ampère equations (11) over finite samples and feature functions, a solution \mathbf{s} to (14) is not guaranteed to yield a unique or optimal map. The *sample-driven* OT problem then, as formulated in [33], is to find a minimum cost map $\nabla \phi_{\mathbf{s}}$ which satisfies sample-equivalence,

$$\min_{\{\nabla \phi_{\mathbf{s}}(X_t^{(j)})\}_{j=1}^J \sim \{w_t^{(j)} X_t^{(j)}\}_{j=1}^J} \sum_{j=1}^J \left\| X_t^{(j)} - \nabla \phi_{\mathbf{s}}(X_t^{(j)}) \right\|^2. \quad (15)$$

Returning to (14), admissible choices of \mathbf{s} in (15) can be identified via root-finding: denote by \mathbf{a} and \mathbf{b} the means of \mathbf{K}_t over the unweighted and weighted reference ensembles,

$$\mathbf{a} = \frac{1}{J} \sum_{j=1}^J \mathbf{K}_t(X_t^{(j)}), \quad \mathbf{b} = \sum_{j=1}^J w_t^{(j)} \mathbf{K}_t(X_t^{(j)}) \in \mathbb{R}^J.$$

For $\mathbf{s} \in \mathbb{R}^J$, define $G : \mathbb{R}^J \rightarrow \mathbb{R}^J$ to be the sample mean of \mathbf{K}_t over $\{\nabla \phi_{\mathbf{s}}(X_t^{(j)})\}_{j=1}^J$,

$$G(\mathbf{s}) = \frac{1}{J} \sum_{j=1}^J \mathbf{K}_t(\nabla \phi_{\mathbf{s}}(X_t^{(j)})) = \frac{1}{J} \sum_{j=1}^J \mathbf{K}_t(X_t^{(j)}) + \mathbf{s}^\top \nabla \mathbf{K}_t(X_t^{(j)}).$$

In order for sample-equivalence to be satisfied, we need to find \mathbf{s}^* such that $G(\mathbf{s}^*) = \mathbf{b}$.

Kuang and Tabak [33] demonstrate that if the Jacobian of G at $\mathbf{s} = \mathbf{0}$

$$\nabla G(\mathbf{s})|_{\mathbf{s}=\mathbf{0}} = \frac{1}{J} \sum_{i=1}^J \nabla \mathbf{K}_t(X_t^{(i)}) \nabla \mathbf{K}_t(X_t^{(i)})^\top \equiv M_t$$

is nonsingular (for which the necessary condition $J \leq dJ$ is automatically satisfied), G is a bijection from a neighborhood U about $\mathbf{s} = \mathbf{0}$ to a neighborhood V about $G(\mathbf{0}) = \mathbf{a}$. If $\mathbf{b} \in V$, then the potential $\phi_{\mathbf{s}}$ parameterized with $\mathbf{s}^* = G^{-1}(\mathbf{b})$ gives the *global minimum* of the sample-based OT problem (15) restricted to maps of the form (12). Furthermore, Kuang and Tabak [33] show that if the kernels are C^2 , then $\phi_{\mathbf{s}^*}$ is locally convex.

For sufficiently small Δt , the system $G(\mathbf{s}^*) = \mathbf{b}$ (14) will be close to linear. Thus, for the sake of efficiency we may approximate \mathbf{s}^* with a single Newton step, setting

$$\mathbf{s}^* \approx - \left(\frac{1}{J} \sum_{i=1}^J \nabla \mathbf{K}_t(X_t^{(i)}) \nabla \mathbf{K}_t(X_t^{(i)})^\top \right)^{-1} \sum_{k=1}^J \left(\frac{1}{J} - w_t^{(k)} \right) \mathbf{K}_t(X_t^{(k)}), \quad (16)$$

to arrive at the update

$$X_{t+\Delta t}^{(j)} = X_t^{(j)} - \left(\nabla_1 K(X_t^{(j)}, X_t^{(1)}) \quad \cdots \quad \nabla_1 K(X_t^{(j)}, X_t^{(J)}) \right) M_t^{-1} \sum_{k=1}^J \left(\frac{1}{J} - w_t^{(k)} \right) \begin{pmatrix} K(X_t^{(k)}, X_t^{(1)}) \\ \vdots \\ K(X_t^{(k)}, X_t^{(J)}) \end{pmatrix},$$

$$j = 1, \dots, J, \quad t \in [0, 1], \quad \{X_0^{(j)}\}_{j=1}^J \stackrel{\text{i.i.d.}}{\sim} \pi_0. \quad (17)$$

Although (17) is distinct from (9) in discrete time, in *continuous* time the two interacting particle systems are equivalent:

Theorem 2 *In the limit $\Delta t \rightarrow 0$, Equation (17) approaches Equation (9). Thus, in the limit $J \rightarrow \infty$ and $\Delta t \rightarrow 0$, the IPS obtained via sample-driven optimal transport (17) approaches the mean-field model (8).*

Proof: See Appendix A.2.

Owing to this equivalence in continuous time, we refer to the interacting particle system (17) as **KFRFlow-Importance (KFRFlow-I)**.

Theorem 2 highlights the fact that linearizing a Monge–Ampère equation for *static* optimal transport between π_t and $\pi_{t+\Delta t}$ results in a Poisson equation, and demonstrates that as $\Delta t \rightarrow 0$ this linearization yields the correct velocity field for the controlled *dynamic* minimum-energy transport problem of Section 3. Furthermore, it elucidates connections between SMC approaches based on tempered self-normalized importance sampling and Fisher–Rao gradient flows.

5 Implementation

KFRFlow (9) can be discretized in time, for example, via the explicit Euler method

$$X_{t+\Delta t}^{(j)} = X_t^{(j)} + \nabla \mathbf{K}_t(X_t^{(j)})^\top M_t^{-1} \frac{\Delta t}{J} \sum_{k=1}^J \left(\log \frac{\pi_1}{\pi_0}(X_t^{(k)}) - \frac{1}{J} \sum_{i=1}^J \log \frac{\pi_1}{\pi_0}(X_t^{(i)}) \right) \mathbf{K}_t(X_t^{(k)}), \quad (18)$$

or any other standard ODE integration scheme, while KFRFlow-I (17) already has the form of a discrete-time iteration. In either case we start from $\{X_0^{(j)}\}_{j=1}^J \stackrel{\text{i.i.d.}}{\sim} \pi_0$ and simulate for unit time to

obtain $\{X_1^{(j)}\}_{j=1}^J \sim \pi_{X_1} \approx \pi_1$. KFRFlow-I (17) and the Euler discretization of KFRFlow (18) are almost identical, and (17) can be recovered, up to multiplication by a constant close to one, from (18) using the approximation $\Delta t \log y = \log y^{\Delta t} \approx y^{\Delta t} - 1$ for $y^{\Delta t} \approx 1$.

In preliminary numerical experiments we have noticed that the matrix M_t in KFRFlow (9) and KFRFlow-I (17) may at times be poorly conditioned, leading to numerical instability or poor quality samples. We have found two tactics to be helpful in mitigating this issue: inflating the diagonal of M_t and introducing noise.

5.1 Regularization of M_t

Issues of ill-conditioning of M_t can be ameliorated by replacing M_t in Equations (17) and (18) with $M_{t,\lambda} = M_t + \lambda I$ for some $\lambda > 0$; this is essentially a Tikhonov regularization of (6) or (16). Inflating the diagonal of M_t does not require additional information about π_1 and π_0 but does require finding an appropriate λ and potentially alters the time-dependent distribution $\rho_t = \text{Law}(X_t)$.

5.2 Stochastic modification

As noted similarly in, e.g., Song et al. [53], Albergo et al. [1], the continuity equation (3) can be written equivalently for any $\epsilon > 0$ as a *Fokker–Planck equation*

$$\partial_t \pi_t = -\nabla \cdot (\pi_t(v_t + \epsilon \nabla \log \pi_t)) + \epsilon \nabla^2 \pi_t, \quad (19)$$

by making use of the identity $\nabla \log \pi_t = \frac{\nabla \pi_t}{\pi_t}$. The Fokker–Planck equation (19) corresponds to an SDE for X_t ,

$$dX_t = (v_t(X_t) + \epsilon \nabla \log \pi_t(X_t)) dt + \sqrt{2\epsilon} dW_t, \quad t \in [0, 1], \quad (20)$$

which possesses the same marginal distributions as the ODE (2). The SDE (20) can hence be used with the velocity field v_t (7) to derive a *stochastic* interacting particle system for traversing the geometric mixture π_t , which we refer to as **Kernel Fisher–Rao Diffusion (KFRD)**; see Appendix B for further details. Simulation of (20) does require access to the score of π_t and hence KFRD is not gradient-free, but in the case that gradients of π_0 and π_1 are available, the score of π_t is simply

$$\nabla \log \pi_t = (1 - t) \nabla \log \pi_0 + t \nabla \log \pi_1.$$

We find that the introduction of noise through (20) often increases numerical stability.

6 Numerical examples

In this section we demonstrate the efficacy of KFRFlow, KFRFlow-I, and KFRD in generating samples from two-dimensional distributions with varying characteristics and on a three funnel distributions in higher dimensions. Additional experimental details may be found in Appendix C. Corresponding code is available at <https://github.com/amaurais/KFRFlow.jl>.

6.1 Two-dimensional Bayesian posteriors

We apply KFRFlow (9) and KFRFlow-I (17) to sample three two-dimensional densities. In all three cases π_1 is a Bayesian posterior proportional to $\pi_0 \ell$ for a likelihood of the form $\ell(x) \propto \exp\left(-\frac{1}{\sigma_\epsilon^2} \|y^* - G(x)\|_2^2\right)$, i.e., $y^* \in \mathbb{R}$ is Gaussian with mean $G(x)$ and variance σ_ϵ^2 . Definitions of the three likelihoods may be found in Appendix C.1.

Figure 2 displays $J = 300$ samples obtained from a forward Euler discretization of KFRFlow with uniform timestep $\Delta t = 0.01$. The samples at $t = 1$ are qualitatively consistent with the target densities for each example.

In Figure 3 we investigate the impact of step-size Δt on the evolution of sample quality, as measured by KSD, with $t \in [0, 1]$. For each example we generate $J = 300$ approximate samples of π_1 with KFRFlow and KFRFlow-I for each $\Delta t \in \{2^{-1}, 2^{-2}, \dots, 2^{-8}\}$ and compute KSD between the samples and π_1 at each step of the iterations. We regularize M_t in the Euler discretization of KFRFlow with λ set to 10^{-1} , 10^{-8} , and 10^{-11} for the donut, butterfly, and spaceships examples but do not regularize M_t in KFRFlow-I. The data plotted in Figure 3 are the result of averaging the values of KSD over 30 repeated trials at each setting of Δt .

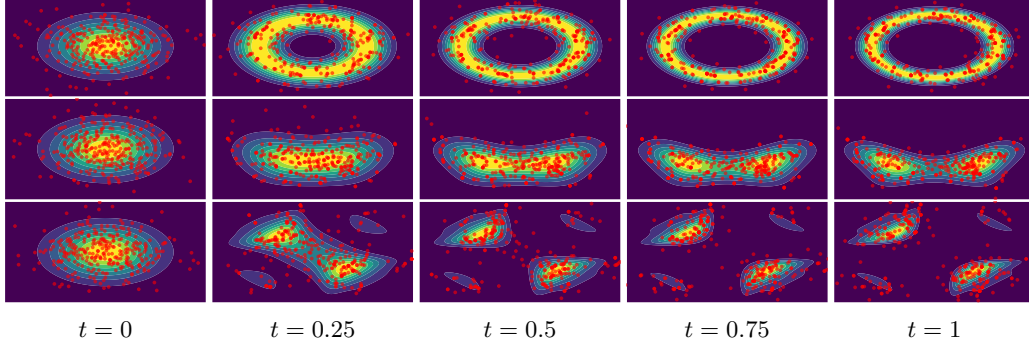


Figure 2: **Two-dimensional posteriors:** samples at $t \in \{0, 0.25, 0.5, 0.75, 1\}$ generated by KFRFlow (9) for the donut (top), butterfly (middle), and spaceships (bottom) examples.

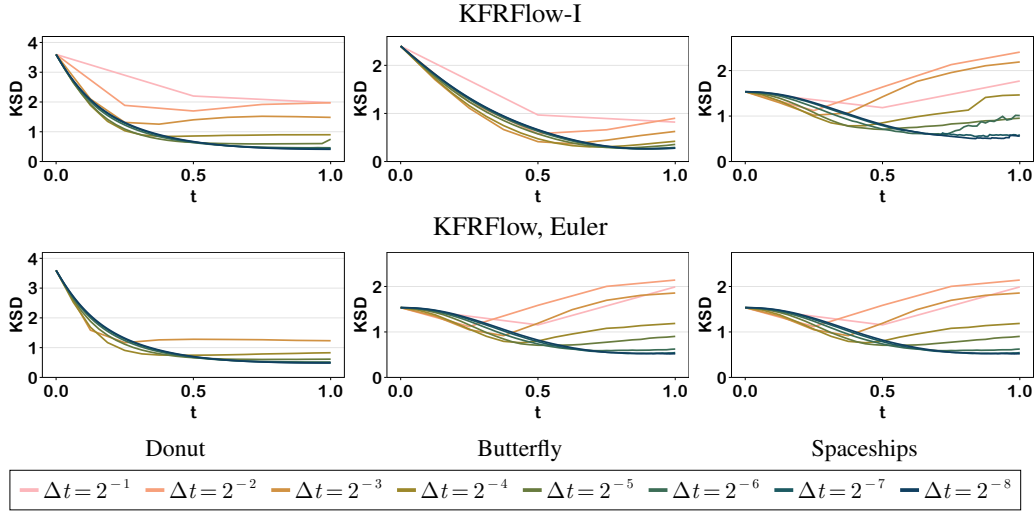


Figure 3: **Two-dimensional posteriors:** KSD as a function of time for KFRFlow-I (top) and an explicit Euler discretization of KFRFlow (bottom) for difference choices of Δt , averaged over 30 repeated trials. In each example Δt must be below a certain threshold to ensure that KSD decreases monotonically throughout the iteration. KFRFlow-I seems to be more stable at large Δt than the Euler discretization of KFRFlow.

In Figures 4 and 5 we compare the sampling performance of KFRFlow, KFRFlow-I, and KFRD to that of Stein variational gradient descent (SVGD) [37], a dynamic sampling algorithm which requires $\nabla \log \pi_1$, and Ensemble Kalman Inversion (EKI) [28], which is gradient-free. We use the algorithms to generate target ensembles of size $J \in \{25, 50, 100, 200, 400\}$ with number of steps $N \in \{2^1, 2^2, \dots, 2^8\}$. As our KFR algorithms and EKI are unit-time, the resulting step-size is $1/N$, but for infinite-time SVGD we must choose a stopping time T , resulting in a step-size of T/N . We test a range of stopping times T for SVGD, regularization levels λ for KFRFlow and KFRFlow-I, and noise levels ϵ for KFRD and report KSD corresponding to the best parameter for each (J, N) . We use a fourth-order Adams–Bashforth discretization (AB4) of KFRFlow because we find that it generates better samples than forward Euler at little additional cost. We use forward Euler with SVGD because we find that it generally performs better than AB4 for SVGD. We use an Euler–Maruyama discretization of for KFRD and EKI. The values of KSD we report are averages over 30 trials.

In Figures 4 and 5 we see that KFRFlow and KFRFlow-I generate better-quality samples than EKI across examples and combinations of (J, N) . There are some settings in the donut example at which EKI and KFRFlow are unstable, but, interestingly, KFRFlow-I is stable across all settings of (J, N) , even in some cases when the gradient-based algorithms KFRD and SVGD are not. We also see that the stochasticity and gradient information in KFRD can yield noticeable improvement over KFRFlow and KFRFlow-I; we see this particularly in the spaceships example for $J = 100$.

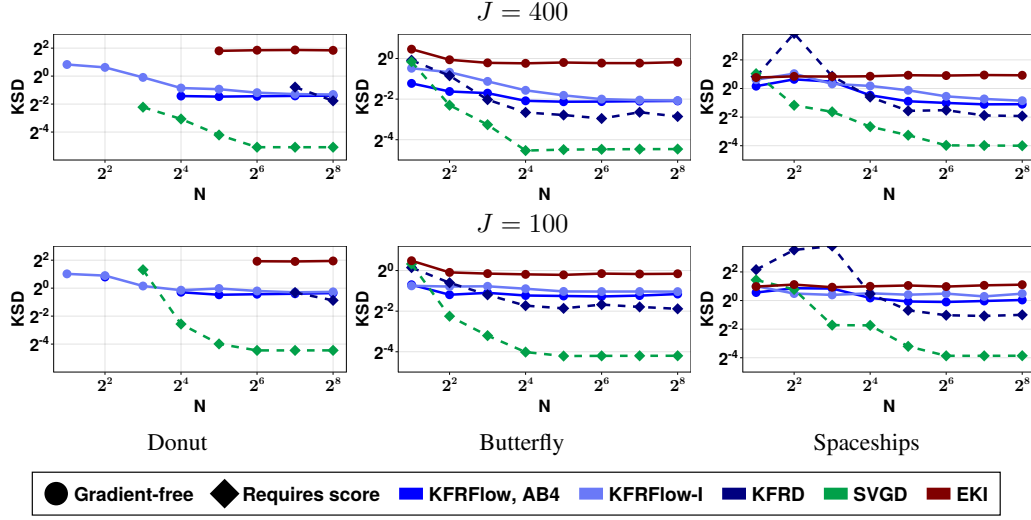


Figure 4: **Two-dimensional posteriors:** average KSD at stopping time between ensembles of size $J = 400$ (top) and $J = 100$ (bottom) generated by KFRFlow, KFRFlow-I, KFRD, EKI, and SVGD as a function of number of steps N . A missing point indicates that a method was unstable at that setting of N .

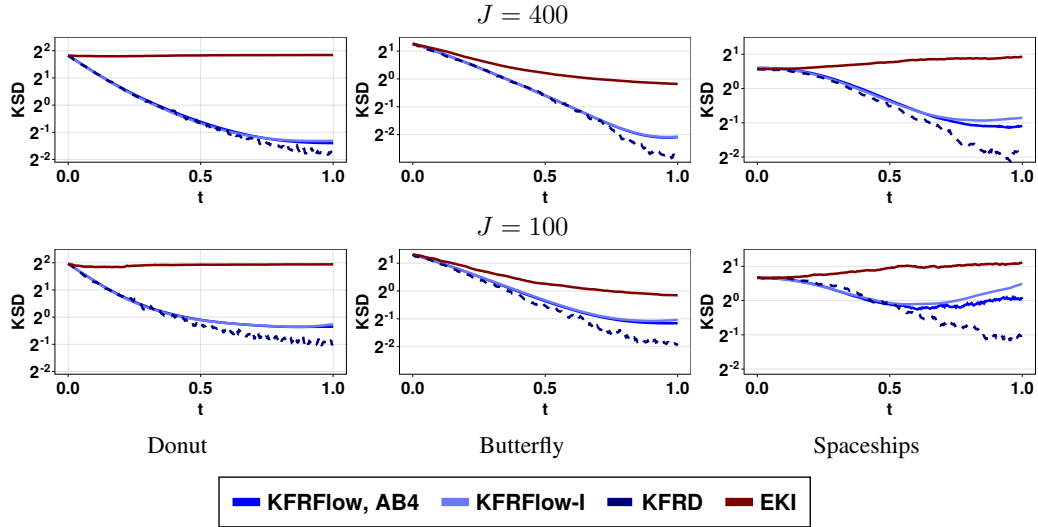


Figure 5: **Two-dimensional posteriors:** evolution of KSD with t for the unit-time methods KFRFlow (AB4), KFRFlow-I, KFRD, and EKI for ensembles of $J = 400$ and $J = 100$ with $\Delta t = 2^{-8}$.

While SVGD is generally the superior sampler for large N , for small N it is often the case that KFRFlow or KFRFlow-I yields comparable or better performance. For additional results and details see Appendix C.

6.2 Higher-dimensional funnel distributions

Here for dimension $d \in \{5, 10, 15\}$ we compare the performance of KFRFlow-I, KFRD, and SVGD in sampling from “funnel” distributions of the form

$$\pi_1(\mathbf{x}) = \mathcal{N}(x_1; 0, 9) \mathcal{N}(\mathbf{x}_{2:d}; \mathbf{0}, \exp(x_1) \mathbf{I}),$$

i.e., X_1 is distributed normally with mean zero and variance nine, and (X_2, \dots, X_d) are multivariate normal with mean zero and covariance matrix $\exp(X_1) \mathbf{I}$. This family of distributions appears in Neal [42] and is a common benchmark for sampling algorithms, e.g., [2, 68, 66].

For each setting of d we apply KFRFlow-I and KFRD (with Euler–Maruyama) to generate $J = 100$ samples from π_1 with $\Delta t = 0.01$. We also apply $N = 1/\Delta t = 100$ steps of SVGD (with forward Euler) to generate the same number of samples. EKI is not applicable to the funnel because it is not a Bayesian posterior with a Gaussian likelihood, and we focus on KFRFlow-I rather than KFRFlow due to its demonstrated stability. The parameters T , λ , and ϵ are optimized by coarse direct search as in Section 6.1; see Appendix C.2 for details. The data in Figure 6 and Figure 7 are reflective of averaging the results of 30 repeated trials.

In Figure 6 we plot KSD between the ensembles as a function of dimension d . We see that KSD increases with dimension for the gradient-based algorithms and that KFRD is competitive with SVGD at all values of d . Interestingly, the quality of the samples generated by the derivative-free KFRFlow-I does not seem to be meaningfully impacted by dimension; a more thorough investigation of this phenomenon, also visible in Figure 7, is an area for future work.

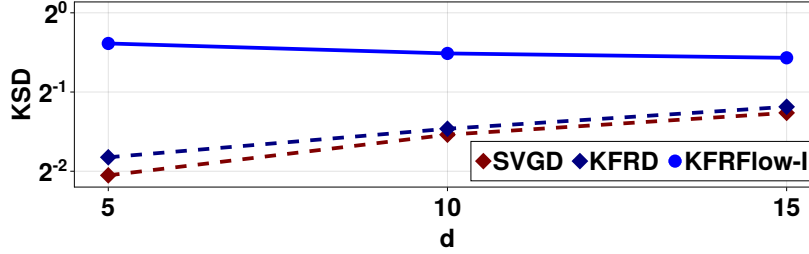


Figure 6: **Funnels:** average KSD at stopping time between samples generated by KFRFlow-I, KFRD, and SVGD for $d \in \{5, 10, 15\}$.

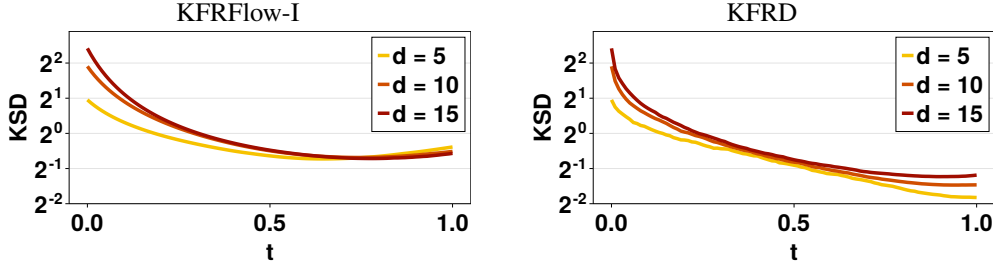


Figure 7: **Funnels:** evolution of KSD with $t \in [0, 1]$ for KFRFlow-I (left) and KFRD (right).

7 Discussion and future work

We have introduced a mean-field ODE model and corresponding interacting particle systems which approximately transport samples from π_0 to π_1 in unit time. We obtain the mean-field ODE by solving an elliptic PDE arising from the Fisher–Rao gradient flow of the negative log likelihood under the ansatz that the solution lies in a reproducing kernel Hilbert space. The RKHS form of the mean-field ODE gives rise to tractable, gradient-free interacting particle systems for sampling. There are several lines of inquiry which would enhance our understanding of the mean-field model and KFRFlow interacting particle systems, chief among them being quantifying approximation error and understanding sample complexity. It would also be interesting to determine whether the kernel approximation applied to the velocity field in our flow gives rise to a notion of kernelized Fisher–Rao geometry for probability measures, similarly to how SVGD can be seen as arising from a gradient flow in a kernelized Wasserstein geometry [19].

Finally, our approach has connections to other sampling algorithms which employ the geometric mixture $\pi_t \propto \pi_0^{1-t} \pi_1^t$ or require solutions of Poisson’s equation, including the feedback particle filter [67, 59] and tempered SMC algorithms [5, 32, 11, 26]. Further exploiting these connections may yield useful modifications and extensions of our current algorithms, related to feature/kernel design, optimal tempering schedules, and beyond.

Acknowledgements

AM and YM were supported by the Office of Naval Research, SIMDA (Sea Ice Modeling and Data Assimilation) MURI, award number N00014-20-1-2595 (Dr. Reza Malek-Madani and Dr. Scott Harper). AM was additionally supported by the NSF Graduate Research Fellowship under Grant No. 1745302.

References

- [1] M. S. Albergo, N. M. Boffi, and E. Vanden-Eijnden, “Stochastic Interpolants: A Unifying Framework for Flows and Diffusions,” no. arXiv:2303.08797, Mar. 2023.
- [2] M. Arbel, A. Matthews, and A. Doucet, “Annealed flow transport monte carlo,” in *International Conference on Machine Learning*. PMLR, 2021, pp. 318–330.
- [3] R. Baptista, B. Hosseini, N. B. Kovachki, and Y. Marzouk, “Conditional Sampling with Monotone GANs: From Generative Models to Likelihood-Free Inference,” no. arXiv:2006.06755, Jun. 2023.
- [4] R. Baptista, Y. Marzouk, and O. Zahm, “On the representation and learning of monotone triangular transport maps,” *Foundations of Computational Mathematics*, vol. in press, 2023, arXiv:2009.10303.
- [5] R. Brekelmans, V. Masrani, T. Bui, F. Wood, A. Galstyan, G. V. Steeg, and F. Nielsen, “Annealed Importance Sampling with q-Paths,” no. arXiv:2012.07823, Dec. 2020.
- [6] Y. Brenier, “Polar factorization and monotone rearrangement of vector-valued functions,” *Communications on pure and applied mathematics*, vol. 44, no. 4, pp. 375–417, 1991.
- [7] M. C. Brennan, D. Bigoni, O. Zahm, A. Spantini, and Y. Marzouk, “Greedy inference with structure-exploiting lazy maps,” *Advances in Neural Information Processing Systems*, vol. 33, pp. 8330–8342, 2020.
- [8] C. Bunne, A. Krause, and M. Cuturi, “Supervised training of conditional Monge maps,” *Advances in Neural Information Processing Systems*, vol. 35, pp. 6859–6872, 2022.
- [9] P. Chen, K. Wu, J. Chen, T. O’Leary-Roseberry, and O. Ghattas, “Projected Stein variational Newton: A fast and scalable Bayesian inference method in high dimensions,” *Advances in Neural Information Processing Systems*, vol. 32, 2019.
- [10] Y. Chen, D. Z. Huang, J. Huang, S. Reich, and A. M. Stuart, “Gradient Flows for Sampling: Mean-Field Models, Gaussian Approximations and Affine Invariance,” Jul. 2023.
- [11] N. Chopin, F. R. Crucinio, and A. Korba, “A connection between tempering and entropic mirror descent,” *arXiv preprint arXiv:2310.11914*, 2023.
- [12] B. Dai and U. Seljak, “Sliced Iterative Normalizing Flows,” in *Proceedings of the 38th International Conference on Machine Learning*. PMLR, Jul. 2021, pp. 2352–2364.
- [13] F. Daum and J. Huang, “Particle flow for nonlinear filters,” in *2011 IEEE International Conference on Acoustics, Speech and Signal Processing (ICASSP)*. IEEE, 2011, pp. 5920–5923.
- [14] —, “Particle flow for nonlinear filters, Bayesian decisions and transport,” in *Proceedings of the 16th International Conference on Information Fusion*. IEEE, 2013, pp. 1072–1079.
- [15] V. De Bortoli, J. Thornton, J. Heng, and A. Doucet, “Diffusion Schrödinger bridge with applications to score-based generative modeling,” in *Advances in Neural Information Processing Systems*, vol. 34. Curran Associates, Inc., 2021, pp. 17 695–17 709. [Online]. Available: <https://proceedings.neurips.cc/paper/2021/hash/940392f5f32a7ade1cc201767cf83e31-Abstract.html>
- [16] P. Del Moral, A. Doucet, and A. Jasra, “Sequential Monte Carlo samplers,” *Journal of the Royal Statistical Society Series B: Statistical Methodology*, vol. 68, no. 3, pp. 411–436, 2006.

- [17] B. M. Dia, “A Continuation Method in Bayesian Inference,” *SIAM/ASA Journal on Uncertainty Quantification*, pp. 646–681, Jun. 2023.
- [18] Z. Ding and Q. Li, “Ensemble Kalman inversion: Mean-field limit and convergence analysis,” *Statistics and Computing*, vol. 31, no. 1, p. 9, Jan. 2021.
- [19] A. Duncan, N. Nüsken, and L. Szpruch, “On the geometry of Stein variational gradient descent,” *Journal of Machine Learning Research*, vol. 24, no. 56, pp. 1–39, 2023.
- [20] D. J. Earl and M. W. Deem, “Parallel tempering: Theory, applications, and new perspectives,” *Physical Chemistry Chemical Physics*, vol. 7, no. 23, pp. 3910–3916, 2005.
- [21] L. C. Evans, “Partial differential equations and Monge-Kantorovich mass transfer,” *Current developments in mathematics*, vol. 1997, no. 1, pp. 65–126, 1997.
- [22] A. Garbuno-Inigo, F. Hoffmann, W. Li, and A. M. Stuart, “Interacting Langevin Diffusions: Gradient Structure and Ensemble Kalman Sampler,” *SIAM Journal on Applied Dynamical Systems*, vol. 19, no. 1, pp. 412–441, Jan. 2020.
- [23] A. Garbuno-Inigo, N. Nüsken, and S. Reich, “Affine Invariant Interacting Langevin Dynamics for Bayesian Inference,” *SIAM Journal on Applied Dynamical Systems*, Jul. 2020.
- [24] C. J. Geyer, “Markov chain Monte Carlo maximum likelihood,” 1991.
- [25] J. Gorham and L. Mackey, “Measuring Sample Quality with Kernels,” Oct. 2020.
- [26] S. Goshtasbpour, V. Cohen, and F. Perez-Cruz, “Adaptive annealed importance sampling with constant rate progress,” in *International Conference on Machine Learning*. PMLR, 2023, pp. 11 642–11 658.
- [27] J. Heng, V. De Bortoli, and A. Doucet, “Diffusion Schrödinger bridges for Bayesian computation,” no. arXiv:2308.14106, Aug. 2023.
- [28] M. A. Iglesias, K. J. H. Law, and A. M. Stuart, “Ensemble Kalman methods for inverse problems,” *Inverse Problems*, vol. 29, no. 4, p. 045001, Apr. 2013.
- [29] P. Jaini, K. A. Selby, and Y. Yu, “Sum-of-squares polynomial flow,” in *International Conference on Machine Learning*. PMLR, 2019, pp. 3009–3018.
- [30] M. Katzfuss and F. Schäfer, “Scalable Bayesian Transport Maps for High-Dimensional Non-Gaussian Spatial Fields,” *Journal of the American Statistical Association*, vol. 0, no. 0, pp. 1–15, 2023.
- [31] I. Kobyzev, S. J. Prince, and M. A. Brubaker, “Normalizing flows: An introduction and review of current methods,” *IEEE transactions on pattern analysis and machine intelligence*, vol. 43, no. 11, pp. 3964–3979, 2020.
- [32] A. Korba and F. Portier, “Adaptive importance sampling meets mirror descent: a bias-variance tradeoff,” in *International Conference on Artificial Intelligence and Statistics*. PMLR, 2022, pp. 11 503–11 527.
- [33] M. Kuang and E. G. Tabak, “Sample-Based Optimal Transport and Barycenter Problems,” *Communications on Pure and Applied Mathematics*, vol. 72, no. 8, pp. 1581–1630, 2019.
- [34] H. R. Künsch, “Recursive Monte Carlo filters: Algorithms and theoretical analysis,” *The Annals of Statistics*, vol. 33, no. 5, pp. 1983 – 2021, 2005. [Online]. Available: <https://doi.org/10.1214/009053605000000426>
- [35] R. S. Laugesen, P. G. Mehta, S. P. Meyn, and M. Raginsky, “Poisson’s equation in nonlinear filtering,” *SIAM Journal on Control and Optimization*, vol. 53, no. 1, pp. 501–525, 2015.
- [36] Y. Lipman, R. T. Q. Chen, H. Ben-Hamu, M. Nickel, and M. Le, “Flow matching for generative modeling,” no. arXiv:2210.02747, 2023. [Online]. Available: <http://arxiv.org/abs/2210.02747>

- [37] Q. Liu and D. Wang, “Stein Variational Gradient Descent: A General Purpose Bayesian Inference Algorithm,” in *Advances in Neural Information Processing Systems*, vol. 29. Curran Associates, Inc., 2016.
- [38] X. Liu, C. Gong, and Q. Liu, “Flow straight and fast: Learning to generate and transfer data with rectified flow,” no. arXiv:2209.03003, 2022. [Online]. Available: <http://arxiv.org/abs/2209.03003>
- [39] Y. Marzouk, T. Moselhy, M. Parno, and A. Spantini, “Sampling via measure transport: An introduction,” *Handbook of uncertainty quantification*, vol. 1, p. 2, 2016.
- [40] A. Myers, A. H. Thiéry, K. Wang, and T. Bui-Thanh, “Sequential ensemble transform for Bayesian inverse problems,” *Journal of Computational Physics*, vol. 427, p. 110055, Feb. 2021.
- [41] R. M. Neal, “Annealed importance sampling,” *Statistics and computing*, vol. 11, pp. 125–139, 2001.
- [42] —, “Slice sampling,” *The annals of statistics*, vol. 31, no. 3, pp. 705–767, 2003.
- [43] A. B. Owen, *Monte Carlo theory, methods and examples*. <https://artowen.su.domains/mc/>, 2013.
- [44] G. Papamakarios, E. Nalisnick, D. J. Rezende, S. Mohamed, and B. Lakshminarayanan, “Normalizing flows for probabilistic modeling and inference,” *The Journal of Machine Learning Research*, vol. 22, no. 1, pp. 2617–2680, 2021.
- [45] C. Rackauckas and Q. Nie, “DifferentialEquations.jl—a performant and feature-rich ecosystem for solving differential equations in Julia,” *Journal of Open Research Software*, vol. 5, no. 1, 2017.
- [46] S. Reich, “A dynamical systems framework for intermittent data assimilation,” *BIT Numerical Mathematics*, vol. 51, no. 1, pp. 235–249, Mar. 2011.
- [47] —, “A Nonparametric Ensemble Transform Method for Bayesian Inference,” *SIAM Journal on Scientific Computing*, vol. 35, no. 4, pp. A2013–A2024, Jan. 2013. [Online]. Available: <http://epubs.siam.org/doi/10.1137/130907367>
- [48] S. Reich and S. Weissmann, “Fokker–Planck Particle Systems for Bayesian Inference: Computational Approaches,” *SIAM/ASA Journal on Uncertainty Quantification*, vol. 9, no. 2, pp. 446–482, Jan. 2021.
- [49] D. Rezende and S. Mohamed, “Variational inference with normalizing flows,” in *International conference on machine learning*. PMLR, 2015, pp. 1530–1538.
- [50] S. Ruchi, S. Dubinkina, and M. A. Iglesias, “Transform-based particle filtering for elliptic Bayesian inverse problems,” *Inverse Problems*, vol. 35, no. 11, p. 115005, Oct. 2019.
- [51] S. Ruchi, S. Dubinkina, and J. de Wiljes, “Fast hybrid tempered ensemble transform filter formulation for Bayesian elliptical problems via Sinkhorn approximation,” *Nonlinear Processes in Geophysics*, vol. 28, no. 1, pp. 23–41, Jan. 2021.
- [52] C. Snyder, T. Bengtsson, P. Bickel, and J. Anderson, “Obstacles to high-dimensional particle filtering,” *Monthly Weather Review*, vol. 136, no. 12, pp. 4629–4640, 2008.
- [53] Y. Song, J. Sohl-Dickstein, D. P. Kingma, A. Kumar, S. Ermon, and B. Poole, “Score-based generative modeling through stochastic differential equations,” in *International conference on learning representations*, 2021.
- [54] A. Spantini, D. Bigoni, and Y. Marzouk, “Inference via low-dimensional couplings,” *The Journal of Machine Learning Research*, vol. 19, no. 1, pp. 2639–2709, 2018.
- [55] A. Spantini, R. Baptista, and Y. Marzouk, “Coupling Techniques for Nonlinear Ensemble Filtering,” *SIAM Review*, vol. 64, no. 4, pp. 921–953, Nov. 2022.

- [56] I. Steinwart and A. Christmann, *Kernels and Reproducing Kernel Hilbert Spaces*. New York, NY: Springer New York, 2008, pp. 110–163. [Online]. Available: https://doi.org/10.1007/978-0-387-77242-4_4
- [57] S. Syed, V. Romaniello, T. Campbell, and A. Bouchard-Côté, “Parallel tempering on optimized paths,” in *International Conference on Machine Learning*. PMLR, 2021, pp. 10 033–10 042.
- [58] A. Taghvaei and B. Hosseini, “An Optimal Transport Formulation of Bayes’ Law for Nonlinear Filtering Algorithms,” in *2022 IEEE 61st Conference on Decision and Control (CDC)*, Dec. 2022, pp. 6608–6613.
- [59] A. Taghvaei and P. G. Mehta, “A survey of feedback particle filter and related controlled interacting particle systems (CIPS),” *Annual Reviews in Control*, vol. 55, pp. 356–378, Jan. 2023.
- [60] G. Trigila and E. G. Tabak, “Data-Driven Optimal Transport,” *Communications on Pure and Applied Mathematics*, vol. 69, no. 4, pp. 613–648, 2016.
- [61] N. G. Trillos, B. Hosseini, and D. Sanz-Alonso, “From Optimization to Sampling Through Gradient Flows,” Feb. 2023.
- [62] F. Vargas, W. Grathwohl, and A. Doucet, “Denoising diffusion samplers,” *arXiv preprint arXiv:2302.13834*, 2023.
- [63] C. Villani, *Topics in Optimal Transportation*. American Mathematical Soc., Aug. 2021.
- [64] L. Wang and N. Nüsken, “Measure transport with kernel mean embeddings,” Jan. 2024.
- [65] C. Xu, X. Cheng, and Y. Xie, “Optimal transport flow and infinitesimal density ratio estimation,” no. arXiv:2305.11857, 2023. [Online]. Available: <http://arxiv.org/abs/2305.11857>
- [66] Z. Xu, N. Chen, and T. Campbell, “Mixflows: principled variational inference via mixed flows,” in *International Conference on Machine Learning*. PMLR, 2023, pp. 38 342–38 376.
- [67] T. Yang, P. G. Mehta, and S. P. Meyn, “Feedback Particle Filter,” *IEEE Transactions on Automatic Control*, vol. 58, no. 10, pp. 2465–2480, Oct. 2013.
- [68] D. Zhang, R. T. Q. Chen, C.-H. Liu, A. Courville, and Y. Bengio, “Diffusion Generative Flow Samplers: Improving learning signals through partial trajectory optimization,” Oct. 2023.

A Proofs

A.1 Proof of Theorem 1

Notice that as $J \rightarrow \infty$ and for any $x \in \mathbb{R}^d$ the sum

$$\frac{1}{J} \sum_{k=1}^J \left(\log \frac{\pi_1}{\pi_0}(X_t^{(k)}) - \sum_{i=1}^J \log \frac{\pi_1}{\pi_0}(X_t^{(i)}) \right) K(X_t^{(k)}, x)$$

approaches the kernelization of $\log \frac{\pi_1}{\pi_0}(\cdot) - \mathbb{E}_{\rho_t}[\log \frac{\pi_1}{\pi_0}]$ with respect to $\rho_t = \text{Law}(X_t)$,

$$K_{\rho_t} \left(\log \frac{\pi_1}{\pi_0}(\cdot) - \mathbb{E}_{\rho_t}[\log \frac{\pi_1}{\pi_0}] \right) (x) \equiv \int_{\mathbb{R}^d} (\log \frac{\pi_1}{\pi_0}(z) - \mathbb{E}_{\rho_t}[\log \frac{\pi_1}{\pi_0}]) K(z, x) d\rho_t(z).$$

Hence, as $J \rightarrow \infty$ the vector

$$\frac{1}{J} \sum_{k=1}^J \left(\log \frac{\pi_1}{\pi_0}(X_t^{(k)}) - \sum_{i=1}^J \log \frac{\pi_1}{\pi_0}(X_t^{(i)}) \right) \begin{pmatrix} K(X_t^{(k)}, X_t^{(1)}) \\ \vdots \\ K(X_t^{(k)}, X_t^{(J)}) \end{pmatrix}$$

can be replaced by the function $x \mapsto K_{\rho_t} \left(\log \frac{\pi_1}{\pi_0}(\cdot) - \mathbb{E}_{\rho_t}[\log \frac{\pi_1}{\pi_0}] \right) (x)$.

Similarly, as $J \rightarrow \infty$, M_t can be viewed as a kernel $M_t : \mathbb{R}^d \times \mathbb{R}^d \rightarrow \mathbb{R}$

$$M_t(z, z') = \mathbb{E}_{X_t \sim \rho_t} \langle \nabla_1 K(X_t, z), \nabla_1 K(X_t, z') \rangle,$$

which can be applied to functions on \mathbb{R}^d as a convolution-type operator with respect to ρ_t ,

$$M_{\rho_t} f(x) = \int_{\mathbb{R}^d} f(z) M_t(x, z) d\rho_t(z) = \iint_{\mathbb{R}^d \times \mathbb{R}^d} f(z) \langle \nabla_1 K(y, x), \nabla_1 K(y, z) \rangle d\rho_t(y) d\rho_t(z).$$

Denoting by $M_{\rho_t}^{-1}$ the inverse operator to M_{ρ_t} , the mean-field limit of (9) can be written

$$\begin{aligned} \dot{X}_t^{(j)} &\xrightarrow{J \rightarrow \infty} \int_{\mathbb{R}^d} \nabla_1 K(X_t^{(j)}, x) M_{\rho_t}^{-1} K_{\rho_t} \left(\log \frac{\pi_1}{\pi_0}(\cdot) - \mathbb{E}_{\rho_t} \left[\log \frac{\pi_1}{\pi_0} \right] \right) (x) d\rho_t(x) \\ &= \mathbb{E}_{X \sim \rho_t} \left[\nabla_1 K(X_t^{(j)}, X) M_{\rho_t}^{-1} K_{\rho_t} \left(\log \frac{\pi_1}{\pi_0}(\cdot) - \mathbb{E}_{\rho_t} \left[\log \frac{\pi_1}{\pi_0} \right] \right) (X) \right]. \end{aligned}$$

A.2 Proof of Theorem 2

Notice that time only enters the update equation (17) through the importance weights $w_t^{(k)}$. To obtain the continuous time limiting ODE we rearrange, divide by Δt on both sides, and take $\Delta t \rightarrow 0$,

$$\lim_{\Delta t \rightarrow 0} \frac{X_{t+\Delta t}^{(j)} - X_t^{(j)}}{\Delta t} = \lim_{\Delta t \rightarrow 0} - \left(\nabla_1 K(X_t^{(j)}, X_t^{(1)}) \quad \dots \quad \nabla_1 K(X_t^{(j)}, X_t^{(J)}) \right) M_t^{-1} \sum_{k=1}^J \frac{\frac{1}{J} - w_t^{(k)}}{\Delta t} \begin{pmatrix} K(X_t^{(k)}, X_t^{(1)}) \\ \vdots \\ K(X_t^{(k)}, X_t^{(J)}) \end{pmatrix}.$$

Examining the terms above involving Δt , we see that for $k \in \{1, \dots, J\}$ we have

$$\begin{aligned} \lim_{\Delta t \rightarrow 0} \frac{\frac{1}{J} - w_t^{(k)}}{\Delta t} &= - \lim_{\Delta t \rightarrow 0} \frac{\frac{(\frac{\pi_1}{\pi_0}(X_t^{(k)}))^{\Delta t}}{\sum_{i=1}^J (\frac{\pi_1}{\pi_0}(X_t^{(i)}))^{\Delta t}} - \frac{1}{J}}{\Delta t} = - \lim_{\Delta t \rightarrow 0} \frac{\frac{(\frac{\pi_1}{\pi_0}(X_t^{(k)}))^{\Delta t}}{\sum_{i=1}^J (\frac{\pi_1}{\pi_0}(X_t^{(i)}))^{\Delta t}} - \frac{(\frac{\pi_1}{\pi_0}(X_t^{(k)}))^0}{\sum_{i=1}^J (\frac{\pi_1}{\pi_0}(X_t^{(i)}))^0}}{\Delta t} \\ &= - \frac{d}{d\Delta t} \frac{(\frac{\pi_1}{\pi_0}(X_t^{(k)}))^{\Delta t}}{\sum_{i=1}^J (\frac{\pi_1}{\pi_0}(X_t^{(i)}))^{\Delta t}} \Big|_{\Delta t=0} \\ &= - \frac{(\frac{\pi_1}{\pi_0}(X_t^{(k)}))^{\Delta t} \log \frac{\pi_1}{\pi_0}(X_t^{(k)}) \sum_{i=1}^J (\frac{\pi_1}{\pi_0}(X_t^{(i)}))^{\Delta t} - (\frac{\pi_1}{\pi_0}(X_t^{(k)}))^{\Delta t} \sum_{i=1}^J (\frac{\pi_1}{\pi_0}(X_t^{(i)}))^{\Delta t} \log \frac{\pi_1}{\pi_0}(X_t^{(i)})}{\left(\sum_{i=1}^J (\frac{\pi_1}{\pi_0}(X_t^{(i)}))^{\Delta t} \right)^2}} \Big|_{\Delta t=0} \\ &= - \frac{J \log \frac{\pi_1}{\pi_0}(X_t^{(k)}) - \sum_{i=1}^J \log \frac{\pi_1}{\pi_0}(X_t^{(i)})}{J^2} = - \frac{1}{J} \left(\log \frac{\pi_1}{\pi_0}(X_t^{(k)}) - \frac{1}{J} \sum_{i=1}^J \log \frac{\pi_1}{\pi_0}(X_t^{(i)}) \right). \end{aligned}$$

Hence, the ODE arising from the limit of (17) as $\Delta t \rightarrow 0$ is (9)

$$\begin{aligned} \dot{X}_t^{(j)} &= \left(\nabla_1 K(X_t^{(j)}, X_t^{(1)}) \quad \dots \quad \nabla_1 K(X_t^{(j)}, X_t^{(J)}) \right) M_t^{-1} \\ &\quad \frac{1}{J} \sum_{k=1}^J \left(\log \frac{\pi_1}{\pi_0}(X_t^{(k)}) - \frac{1}{J} \sum_{i=1}^J \log \frac{\pi_1}{\pi_0}(X_t^{(i)}) \right) \begin{pmatrix} K(X_t^{(k)}, X_t^{(1)}) \\ \vdots \\ K(X_t^{(k)}, X_t^{(J)}) \end{pmatrix}, \end{aligned}$$

with initial condition $\{X_0^{(j)}\}_{j=1}^J \stackrel{\text{i.i.d.}}{\sim} \pi_0$. Thus, by Theorem 1, the mean-field, continuous-time limit of (17) is (8).

B Kernel Fisher–Rao Diffusion

The continuity equation (3) which we solve for the velocity v_t can equivalently be written for any $\epsilon > 0$ as a *Fokker–Planck equation*

$$\partial_t \pi_t = -\nabla \cdot (\pi_t (v_t + \epsilon \nabla \log \pi_t)) + \epsilon \nabla^2 \pi_t,$$

corresponding to the SDE

$$dX_t = (v_t(X_t) + \epsilon \nabla \log \pi_t(X_t)) dt + \sqrt{2\epsilon} dW_t, \quad t \in [0, 1]. \quad (21)$$

This SDE possesses the same marginal distributions as the ODE (2). Using the same interacting particle approximation for the mean-field velocity v_t (8) that we use to define deterministic KFRFlow (9), we can also define a *stochastic* interacting particle system for approximately traversing the geometric mixture $\pi_t \propto \pi_0^t \pi_1^{1-t}$,

$$\begin{aligned} dX_t^{(j)} = & \nabla \mathbf{K}_t(X_t^{(j)})^\top M_t^{-1} \frac{1}{J} \sum_{k=1}^J \left(\log \frac{\pi_1}{\pi_0}(X_t^{(k)}) - \frac{1}{J} \sum_{i=1}^J \log \frac{\pi_1}{\pi_0}(X_t^{(i)}) \right) \mathbf{K}_t(X_t^{(k)}) dt \\ & + \epsilon \nabla \log \pi_t(X_t^{(j)}) dt + \sqrt{2\epsilon} dW_t, \end{aligned} \quad (22)$$

where we have used the notation $\mathbf{K}_t(\cdot) = (K(\cdot, X_t^{(1)}), \dots, K(\cdot, X_t^{(J)}))^\top$ and $\nabla \mathbf{K}_t \in \mathbb{R}^{J \times d}$ is the Jacobian of \mathbf{K}_t . It follows directly from Theorem 1 that the mean-field limit of (22) is the SDE (21) with v_t as in (8). Because we know $\pi_t \propto \pi_0^{1-t} \pi_1^t$ explicitly, the score of π_t can be computed directly as $\nabla \log \pi_t = (1-t) \nabla \log \pi_0 + t \nabla \log \pi_1$. We refer to the interacting particle system (22) as **Kernel Fisher–Rao Diffusion (KFRD)** and note that it can be simulated with any off-the-shelf SDE solver, for example Euler–Maruyama.

C Experimental details and additional numerical results

Across all experiments we take the kernel $K(\cdot, \cdot)$ to be inverse multiquadric (IMQ)

$$K(x, x') = \left(1 + \frac{\|x - x'\|^2}{h^2}\right)^{-1/2} \quad (23)$$

with bandwidth $h > 0$ selected at each step of the iterations according to the median heuristic [37]. We use this same kernel and median heuristic bandwidth with SVGD in our comparison experiments. We assess sample quality using Kernel Stein Discrepancy (KSD) [25] with the IMQ kernel (23) with bandwidth $h = 1$. The reference distribution π_0 is always taken to be standard Gaussian. We perform all experiments in Julia using the package `DifferentialEquations.jl` [45] to integrate the ODEs and SDEs associated with KFRFlow, KFRD, SVGD, and EKI.

C.1 Two-dimensional Bayesian posteriors

C.1.1 Experimental setup

We apply KFRFlow (9) and KFRFlow-I (17) to sample three two-dimensional densities. In all three cases π_1 is a Bayesian posterior proportional to $\pi_0 \ell$ for a likelihood $\ell = \pi(y^* | \cdot)$ of the form

$$\ell(x) \propto \exp\left(-\frac{1}{\sigma_\epsilon^2} \|y^* - G(x)\|_2^2\right),$$

i.e., $y^* \in \mathbb{R}$ is Gaussian with mean $G(x)$ and variance σ_ϵ^2 . Definitions of the three likelihoods and descriptions of the deformation behavior they entail may be found in Table 1.

Table 1: Likelihoods for the two-dimensional Bayesian example problems

| $G(x)$ | y^* | σ_ϵ^2 | Behavior | Nickname |
|---------------------------------|-------|---------------------|---------------|------------|
| $\sqrt{x_1^2 + x_2^2}$ | 2 | 0.25 ² | Concentration | Donut |
| $\sin(x_2) + \cos(x_1)$ | -1 | 0.6 ² | Bimodality | Butterfly |
| $\sin(x_1 x_2) + \cos(x_1 x_2)$ | -1 | 0.5 ² | Multimodality | Spaceships |

We compare we compare the sampling performance of KFRFlow, KFRFlow-I, and KFRD to that of SVGD [37] and EKI [28]. We use the algorithms to generate target ensembles of size $J \in \{25, 50, 100, 200, 400\}$ with number of steps $N \in \{2^1, 2^2, \dots, 2^8\}$. As our KFR algorithms and EKI are unit-time, the resulting step-size is $1/N$, but infinite-time SVGD we must choose a stopping time T , resulting in a step-size of T/N . We test values of $T \in \{5, 10, 15, 20, 25\}$ and for each combination of (J, N) report the results corresponding to the best-performing T . Similarly, for KFRFlow and KFRFlow-I we test regularization level $\lambda \in \{0, 10^{-1}, 10^{-2}, \dots, 10^{-8}\}$ and for KFRD we test noise level $\epsilon \in \{10^{-4}, 10^{-3}, \dots, 10^1\}$ and report KSD corresponding to the best parameter for each (J, N) . The optimal parameters for each combination of (J, N) can be seen in Figure 8.

We use a fourth-order Adams–Bashforth discretization (AB4) of KFRFlow because we find that it generates higher-quality samples than forward Euler at little additional computational cost. We use forward Euler for SVGD because we find that it is generally made worse by AB4. For comparisons of the sampling performance of these different ODE discretization methods see Figures 9 and 10. We use an Euler–Maruyama discretization of for KFRD and EKI.

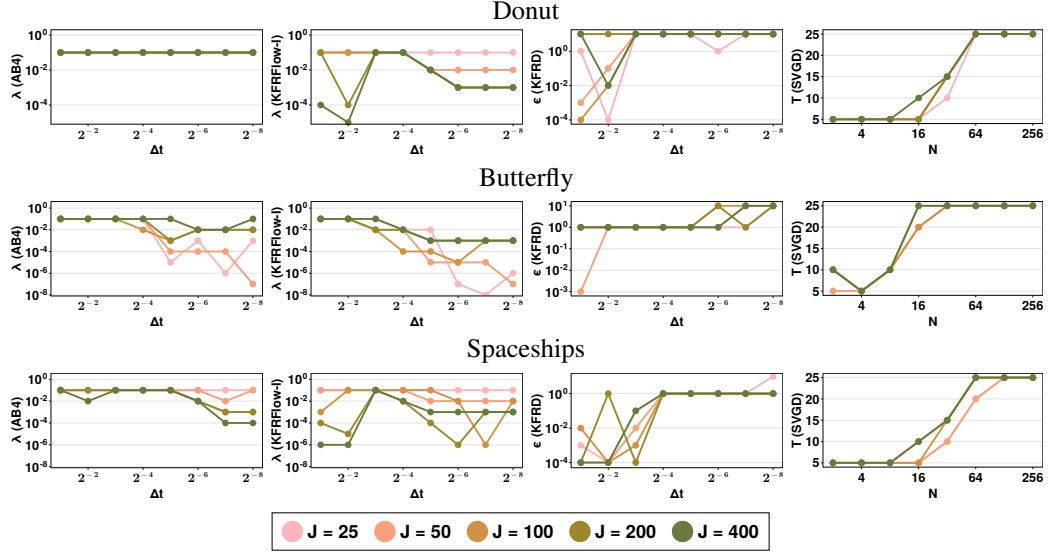


Figure 8: Optimal parameter choices for KFRFlow (left), KFRFlow-I (second from left), KFRD (third from left), and SVGD (right) for the donut (top), butterfly (middle), and spaceships (bottom) examples.

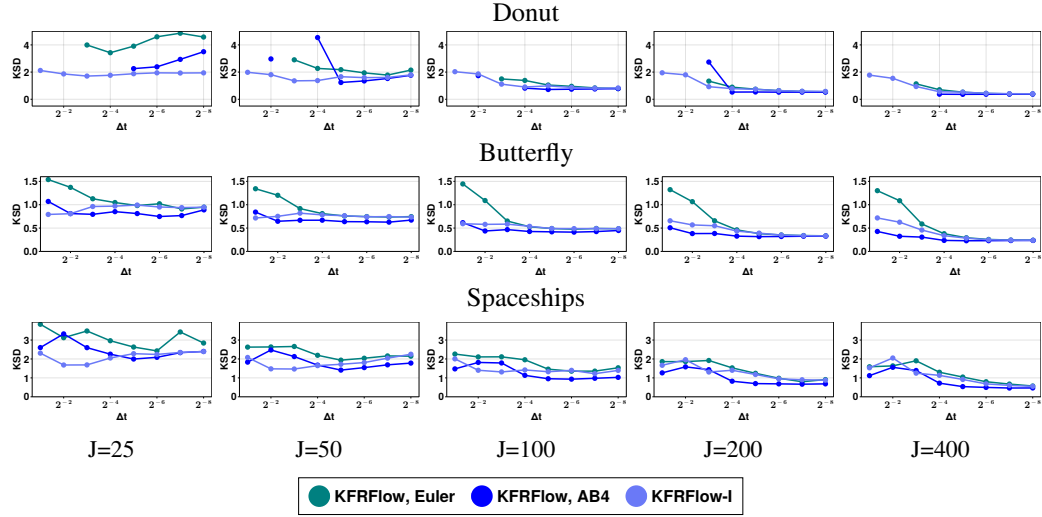


Figure 9: **Two-dimensional posteriors:** Mean KSD of ensembles generated by forward Euler and AB4 discretizations of KFRFlow and KFRFlow-I for varying ensemble size and Δt . KFRFlow-I and the AB4 discretization of KFRFlow generally out-perform the forward Euler discretization of KFRFlow.

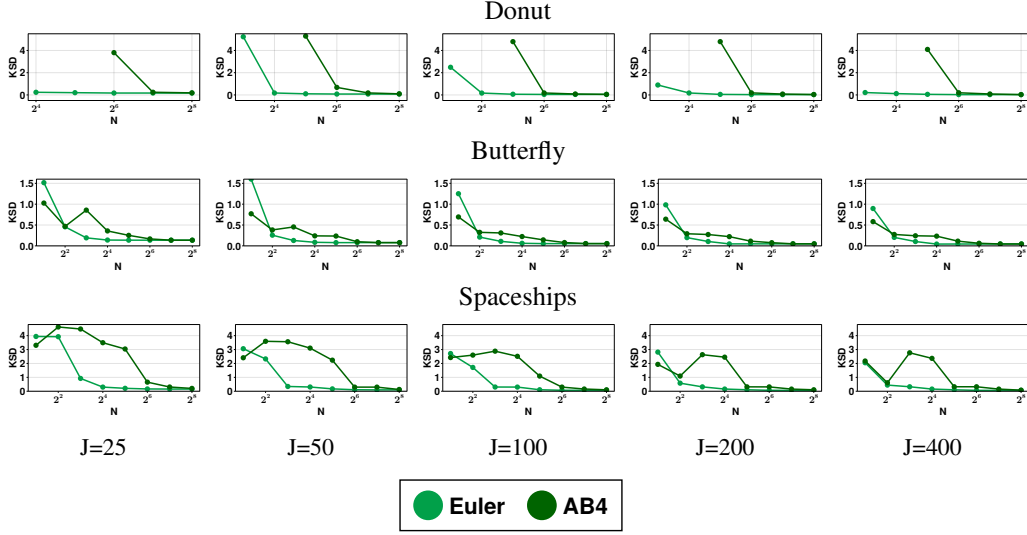


Figure 10: **Two-dimensional posteriors:** Mean KSD of ensembles generated by forward Euler and AB4 discretizations of SVGD. Using AB4 in place of forward Euler with SVGD tends only to make sample quality worse.

C.1.2 Additional results

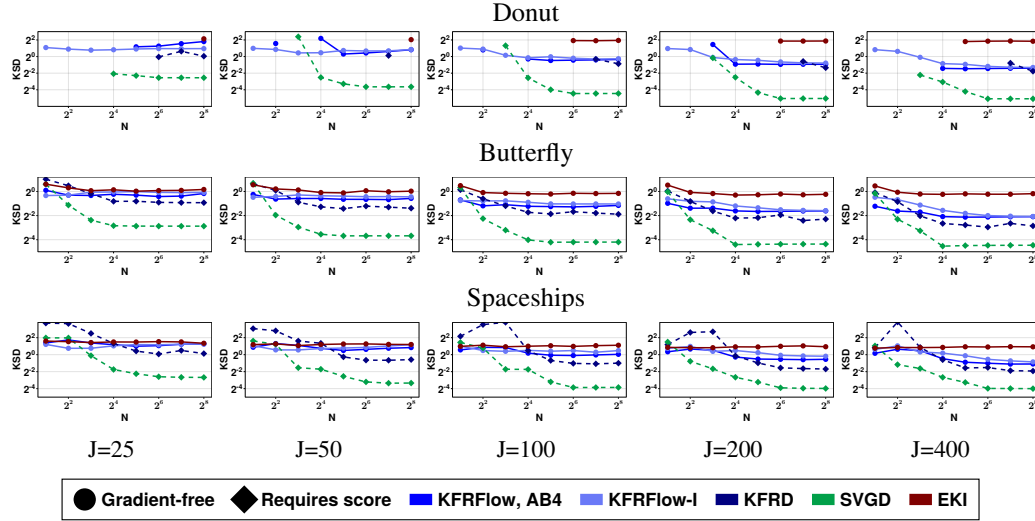


Figure 11: **Two-dimensional posteriors:** average KSD at stopping time between ensembles of size $J \in \{25, 50, 100, 200, 400\}$ generated by KFRFlow, KFRFlow-I, KFRD, EKI, and SVGD as a function of number of steps N . A missing point indicates that a method was unstable at that setting of N .

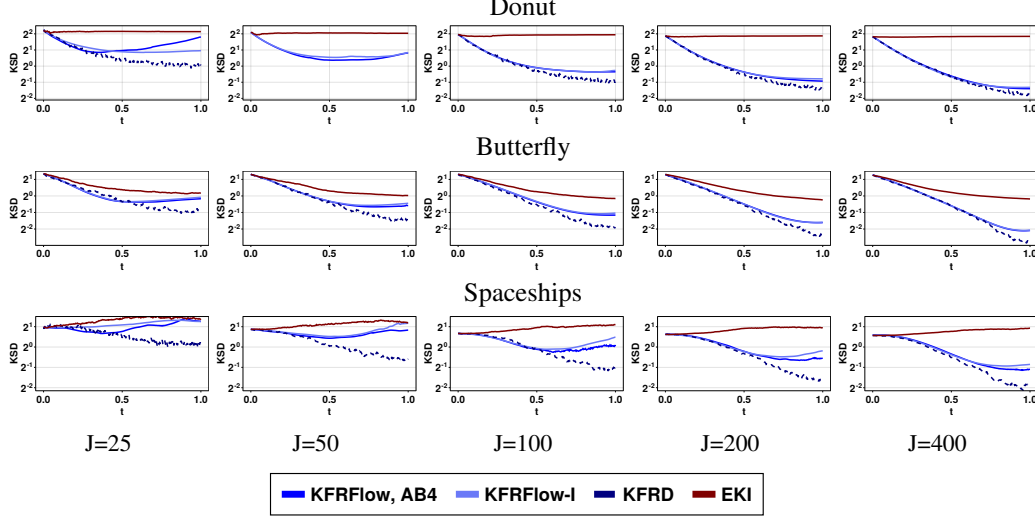


Figure 12: **Two-dimensional posteriors:** evolution of KSD with $t \in [0.1]$ for the unit-time methods KFRFlow (AB4), KFRFlow-I, KFRD, and EKI for ensembles of $J \in \{25, 50, 100, 200, 400\}$ with $\Delta t = 2^{-8}$.

C.2 Higher-dimensional funnels

For dimension $d \in \{5, 10, 15\}$ we compare the performance of KFRFlow-I, KFRD, and SVGD in sampling from “funnel” distributions of the form

$$\pi_1(\mathbf{x}) = \mathcal{N}(x_1; 0, 9) \mathcal{N}(\mathbf{x}_{2:d}; \mathbf{0}, \exp(x_1) \mathbf{I}),$$

i.e., X_1 is distributed normally with mean zero and variance nine, and (X_2, \dots, X_d) are multivariate normal with mean zero and covariance matrix $\exp(X_1) \mathbf{I}$. This family of distributions appears in [42] and is commonly used as a benchmark for sampling algorithms, e.g., [2, 68, 66].

For each setting of d we apply KFRFlow-I and KFRD (with Euler–Maruyama) to generate $J = 100$ samples from π_1 with $\Delta t = 0.01$. We also apply $N = 1/\Delta t = 100$ steps of SVGD (with forward Euler) to generate the same number of samples. For KFRFlow-I we tested values of the regularization parameter $\lambda \in \{10^{-2}, 10^{-3}, 10^{-4}\}$ and found that $\lambda = 10^{-3}$ corresponded to the highest quality samples; similarly, we tested noise levels $\epsilon \in \{1.0, 2.5, 5.0, 10.0\}$ for KFRD and stopping times $T \in \{25, 50, 100\}$ for SVGD, finding that $\epsilon = 2.5$ and $T = 100$ performed best. The data in Figure 6 and Figure 7 were generated with these settings of λ , ϵ , and T and are reflective of averaging KSD values for each algorithm over 30 repeated trials.